The Astronomical Journal, 125:1897–1907, 2003 April

ARP 194: EVIDENCE OF TIDAL STRIPPING OF GAS AND CROSS-FUELING

P. Marziani,[1] D. Dultzin-Hacyan,[2] M. D'Onofrio,[3] and J. W. Sulentic[4]

Received 2002 May 23; accepted 2002 December 18

ABSTRACT

We present new imaging and spectroscopic observations of the interacting system Arp 194 (≡UGC 6945 ≡ VV 126). The northern component (A194N) is a distorted spiral or ring galaxy likely disrupted by a collision or close encounter with a southern galaxy (A194S). There is evidence that a third galaxy with similar recession velocity is projected on A194N, but its role is likely secondary. A194S is connected to A194N by a string of emission knots, which motivates our interpretation that the former was the intruder. Three of the knots are easily discernible in *B*, *R*, and Hα images and are assumed to trace the path of the intruder following the encounter, which we estimate occurred a few times 10^8 yr ago. Both A194S and A194N are experiencing strong bursts of star formation: the Hα luminosity indicates a total star formation rate $\sim$10 $M_\odot$ yr^{-1}. The lack of detectable *J* and *K* emission from the blobs, along with strong Hα emission, indicates that an evolved stellar population is not likely to be present. The brightest knot (closest to A194S) shows a star formation rate of $\approx$1.2 $M_\odot$ yr^{-1}, which, if sustained over a time $\approx 7 \times 10^7$ yr, could explain the spectral energy distribution. This suggests that the stripped matter was originally predominantly gaseous. The brightest knot is detected as a FIRST radio source, and this is likely the signature of supernova remnants related to enhanced star formation. Motions in the gas between the brightest knot and A194S, traced by an emission line link of increasing radial velocity, suggests infall toward the center of the intruder. Arp 194 is therefore one of the few galaxies where evidence of "cross-fueling" is observed.

Key words: galaxies: individual (Arp 194) — galaxies: interactions — galaxies: kinematics and dynamics — galaxies: nuclei — galaxies: starburst

1. INTRODUCTION

Arp 194 (Arp 1966; UGC 6945 ≡ VV 126; Vorontsov-Velyaminov 1977) is a small angular size system of two major components: a northwestern galaxy of disrupted morphology ($0\rlap{.}'8 \times 0\rlap{.}'6$; see Figs. 1 and 2) and an apparently more regular galaxy ($0\rlap{.}'35 \times 0\rlap{.}'35$) located $\approx 40''$ to the southeast. From the heliocentric velocity of the Arp 194S (hereafter A194S), $v_r \approx 10{,}500$ km s^{-1} (see § 3), we infer a distance of 175 Mpc for the system ($H_0 \approx 60$ km s^{-1} Mpc^{-1}). Arp 194N and Arp 194S are therefore separated by a projected linear distance $d_p \approx 34$ kpc ($1''$ corresponds to $d_p \approx 850$ pc). Arp described the Arp 194 system as belonging to the class of "galaxies with material ejected from nuclei." Arp noted further "outer material connected by thin filament to very hard nucleus." Several peculiar features of Arp 194N (A194N) have also been discussed in an early study (Metlov 1980).

Theoretical modeling involving a reliable treatment of dissipative phenomena like star formation, as well as high-resolution numerical simulations of stellar and gas motions, are still the current frontier in our understanding of interacting galaxies (see, e.g., Hearn & Lamb 2001; Semelin & Combes 2000; Barnes & Hernquist 1998, 1996; Mihos & Hernquist 1996). From simulations, we expect a wide range of phenomenological properties due to interaction. Gravitational forces can marginally enhance the star formation rate (SFR) in an unbound intergalactic encounter as well as give rise to the most luminous bursts of star formation observed in merging systems (see, e.g., Krongold, Dultzin-Hacyan, & Marziani 2002 and references therein). Tidal effects drive noncircular motion in disk galaxies, can strip a significant amount of stars and gas, and even lead to the formation of the so-called tidal dwarf galaxies (Barnes & Hernquist 1992). A related issue is the role of gravitational interaction in fueling nonthermal nuclear activity. Both simulations and observations of single interacting systems are a necessary complement to statistical studies on the frequency of interacting systems among active galaxies, since the latter provide valuable but only circumstantial evidence in favor of interaction as a major driver of nuclear activity (Krongold et al. 2002; see, however, Schmitt 2001 and references therein). Collisional ring galaxies are excellent laboratories for studying galactic evolution, global star formation, and the occurrence of gas cross-fueling among galaxies. The prototype of this class of objects is the Cartwheel galaxy, A0035−33. Only few systems similar to this object are known: among the best studied we recall VII Zw 466, Arp 10, II Zw 28, II Hz 4, A76, LT 36, NGC 985, and LT 41 (Appleton & Marston 1997). Other likely cases are Arp 119 (Hearn & Lamb 2001), Arp 118 (Charmandaris et al. 2001), Arp 284 (Smith & Wallin 1992; Smith, Struck, & Pogge 1997), and Arp 143 (Appleton, Schombert, & Robson 1992). The dominant ring morphology is thought to result from a head-on collision between two galaxies, one of which traveled close to the spin axis of the other, striking the disk close to its center. The resulting gravitational perturbation is believed to drive a set of symmetric waves or caustics through the stellar disk (Lynds & Toomre 1976; Theys &

[1] Osservatorio Astronomico di Padova, Istituto Nazionale di Astrofisica, vicolo dell'Osservatorio 5, I-35122 Padova, Italy; marziani@pd.astro.it.

[2] Instituto de Astronomía, Universidad Nacional Autonoma de México, 04510 México, D.F., Mexico; deborah@astroscu.unam.mx.

[3] Dipartimento di Astronomia, Università di Padova, Vicolo dell'Osservatorio 2, I-35122 Padova, Italy; donofrio@pd.astro.it.

[4] Department of Physics and Astronomy, University of Alabama, Tuscaloosa, AL 35487; giacomo@merlot.astr.ua.edu.

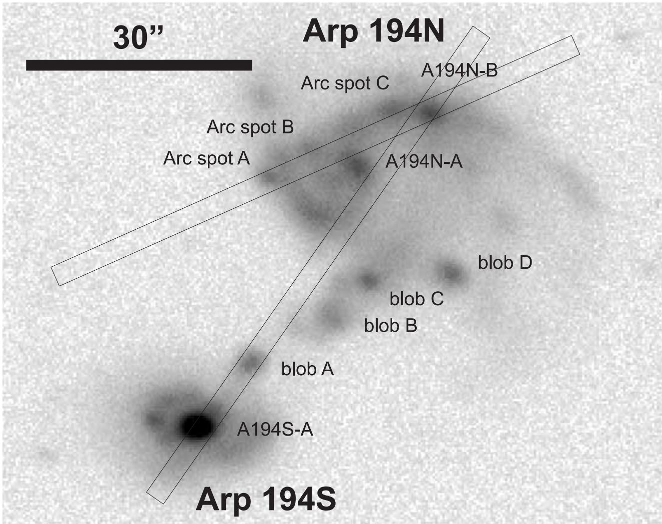

FIG. 1.—Morphological details of the Arp 194 system and their identification. The slit position (P.A. = 145° and P.A. = 118°) and width (2."6) is shown on scale. North is to the top, and east to the left. Uncertainty in the placement of the slit is estimated to be within ±0."5.

TABLE 1
LOG OF SPM OBSERVATIONS

Date Obs.	UT[a]	ET[b]	P.A. (deg)	Filter/Sp. Range
1995 Jan 30	11 31	600	n. a.	R
1995 Jan 30	11 47	600	n. a.	R
1995 Jan 30	12 05	600	n. a.	R
1995 Jan 30	12 19	600	n. a.	R
1995 Jan 30	12 33	900	n. a.	Hα+[N II]
1995 Jan 30	12 50	900	n. a.	Hα+[N II]
1995 Jan 30	13 07	900	n. a.	Hα+[N II]
1995 Jan 31	09 34	600	n. a.	R
1995 Jan 31	09 46	900	n. a.	B
1995 Jan 31	10 03	900	n. a.	B
1995 Jan 31	10 27	900	n. a.	B
1995 Feb 2......	11 54	1800	145	6165–7246 Å
1995 Feb 2......	12 25	1800	145	6165–7246 Å
1995 Feb 2......	13 04	1800	118	6165–7246 Å
1995 Feb 2......	13 32	1800	118	6165–7246 Å

[a] Universal Time in hours and minutes at exposure start.
[b] Exposure time duration in seconds for each single frame.

Spiegel 1976; Toomre 1978; Appleton & Struck-Marcell 1987; Struck-Marcell 1990). Computer simulations of such head-on encounters, in which at least one galaxy has a significant gaseous component, show indeed the production of density enhancements and shock waves in the interstellar medium. These high-density regions coincide with the location of recent, large-scale star formation observed in ring galaxies.

Figures 1 and 2 suggest that A194N is a collisionally induced ring galaxy connected to the past intruder A194S by a string of relatively bright knots (§ 3). Several photometric properties indicate star formation rates typical of starburst galaxies (§ 3.5). The surprisingly strong radio emission from A194S and knot A is likely due mainly to supernova remnants, which implies even higher star formation rates (§ 3.5.4) and substantial internal obscuration. Relatively rare systems, such as Arp 194, where gas motions are induced by a head-on encounter, enable us to unambiguously infer the geometry of the system. In this case that information provides evidence for "cross-fueling" (see § 4.1). Our results for Arp 194 have intriguing implications on the analysis and interpretation of galactic superwinds (§ 4).

2. OBSERVATIONS, DATA REDUCTION, AND ANALYSIS

Johnson (B, R) and narrowband (Hα) images of Arp 194 were obtained at the Cassegrain focus of the 2.1 m telescope of the Observatorio Astronómico Nacional de México at San Pedro Martir (SPM) on 1995 January 30–31. The detector was a Tektronik CCD (24 μm square pixel size, 1024 × 1024 format) that yielded a scale of 0."315 pixel^{-1} and a field of view of 5.'4. A narrowband filter with $\lambda_C \approx 6819$ Å, and $\Delta\lambda \approx 86$ Å allowed coverage of the Hα+[N II] $\lambda\lambda$6548, 6583 blend of Arp 194 (§ 3.1). Table 1 provides a log of each single exposure taken at SPM.

Long-slit spectra were obtained on 1995 February 2 at the 2.1 m telescope equipped with a Boller & Chivens spectrograph. A 1200 line mm^{-1} grating was employed for observations of the Hα spectral region (coverage ≈ 6170–7240 Å). Four spectrograms were taken, two at position angle P.A. ≈ 145° and two P.A. ≈ 118°, with an exposure time totaling 60 minutes at each P.A. (see Fig. 1 for slit placement). The slit was opened to 200 μm (2."6 on the focal plane of the telescope). This setup resulted in a resolution of ≈2.5 Å FWHM (≈110 km s^{-1} at redshifted Hα). The data reduction for both imaging and spectroscopic data and the calibration procedure followed standard IRAF practice and has been identical to that employed by Marziani et al. (1999), who used data obtained during the same nights. We will not describe them again here.

3. RESULTS

3.1. *Morphology and Photometry*

The morphology of the Arp 194 system in the B band is shown in Figure 1, where some of the most prominent features are identified. A multifrequency view is provided in Figure 2. The four panels show (*clockwise from top left*) the SPM B-band image (with a cut optimized to show the internal structure at the expense of loss of the fainter envelope), the continuum subtracted Hα+[N II] $\lambda\lambda$6548, 6583 narrowband image, the $B-R$ color index map, and the radio map at 1.4 GHz obtained from the FIRST survey (Becker, White, & Helfand 1995). Table 2 reports the photometric properties of the main features visible in these maps. The uncertainty in the B and R photometry is estimated to be ≈±0.05 mag at a 2 σ confidence level. $B-R$ values are therefore accurate within $\lesssim$0.1 mag. The uncertainty associated to the overall Hα+[N II] $\lambda\lambda$6548, 6583 calibration is estimated to be within 10%. Due to the diffuse nature of large part of Hα emission, an appropriate uncertainty is probably a factor 2 for the measurements on the faintest and most diffuse regions, while it should be within 20% for the brightest and least diffuse ones. A194S is a surprisingly strong radio source when compared to nearby Seyfert galaxies. The specific power of A194S is log $P_{\nu,1.4\mathrm{GHz}} \approx 22.1$, with $P_{\nu,1.4\mathrm{GHz}}$ in W Hz^{-1}), placing it at the high end of the distribution of

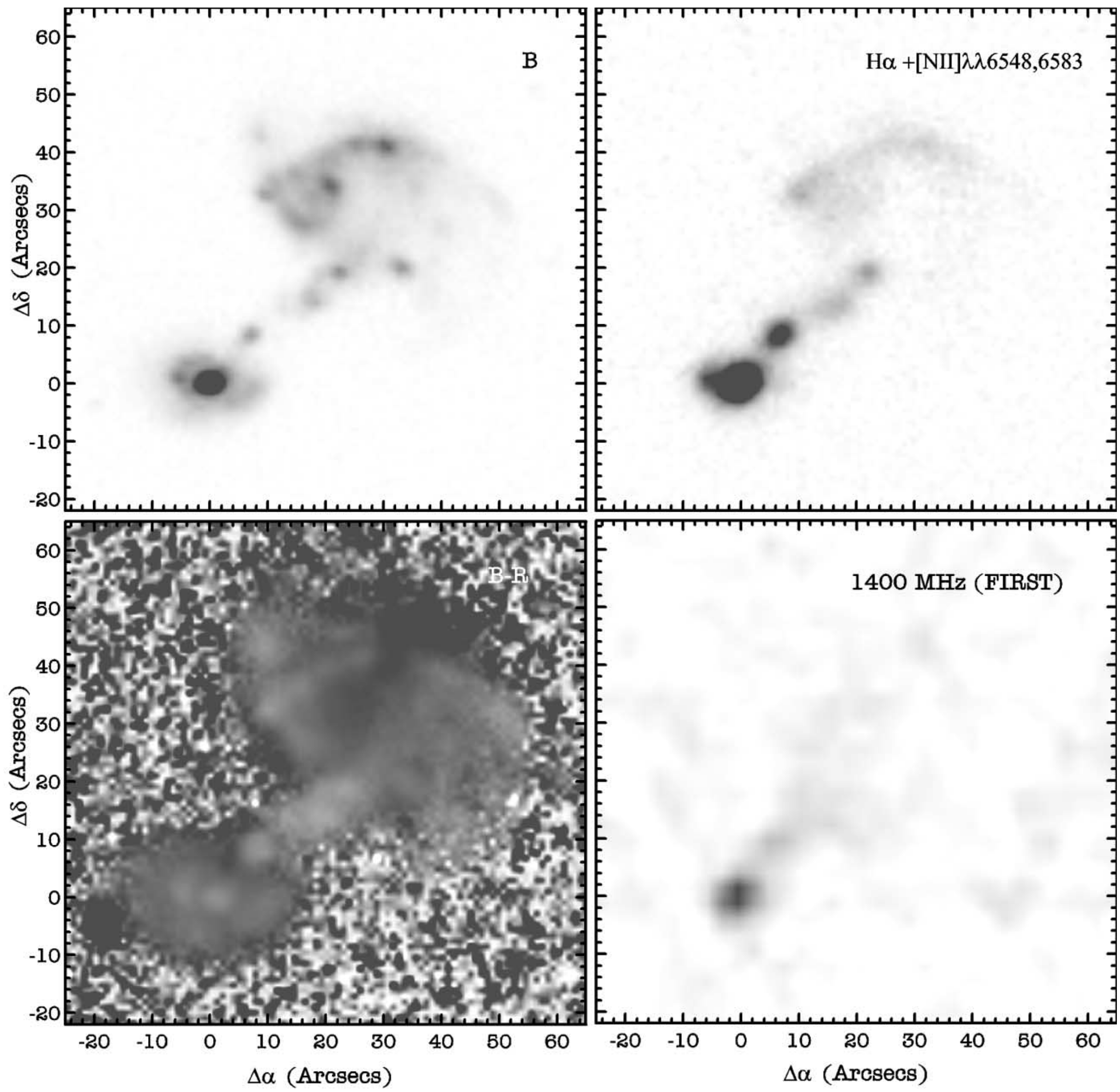

FIG. 2.—Multifrequency morphology of the Arp 194 system. *Top left*: Johnson *B* image. *Top right*: Continuum-subtracted narrowband image [Hα+[N II] $\lambda\lambda$6548, 6583]. *Bottom left*: $B-R$ color map. Limits on scale are -1.2 (*white*) and 1.2 (*black*). *Bottom right*: Radio emission at 1.4 GHz from FIRST data. In all panels north is to the top, and east to the left.

radio power in Palomar Seyferts, which cover the range $\log P_{\nu,1.4\mathrm{GHz}} \approx 18$–22 (Ulvestad & Ho 2001; Ho & Ulvestad 2001). Of course, this is still negligible compared to nearby radio galaxies such as NGC 1275 with $\log \nu P_{\nu,1.4\mathrm{GHz}} \approx 25.6$ (Owen, Spanger, & Cotton 1980).

Another remarkable feature of this system is a string of relatively bright knots ("blobs") in between the two components of Arp 194, aligned along the north western direction (the "streamers" in the terminology of Metlov 1980). The blobs B and C have $B-R \approx 0.12$ and 0.26, respectively. In Table 2 the *J* and *K* magnitudes are upper limits from the isophotal contours published by Bushouse & Stanford (1992). The blobs are not present at the lowest contour levels traced by these authors. The trail of blobs between A194S and A194N can be readily interpreted as stripped gas due to the interpenetrating encounter between A194S and A194N (see Marziani et al. 1994; Horellou & Combes 2000). There are several lines of evidence in favor of this interpretation:

1. The rough alignment of the three main blobs observed in between A194S and A194N. The blobs literally provide a trail of "footprints" tracing the path of the intruding galaxy (A194S) after crossing A194N. They identify a direction pointing close to the geometrical center of A194N.

2. The lack of any *K* counterpart for all blobs, which suggests a common origin for the blobs. In particular, it rules out that blob A is a background galaxy.

3. Almost no solution of continuity nor any radial velocity discontinuity Hα emission in the two-dimensional spectra at P.A. 145° (see Fig. 3 and § 3.3).

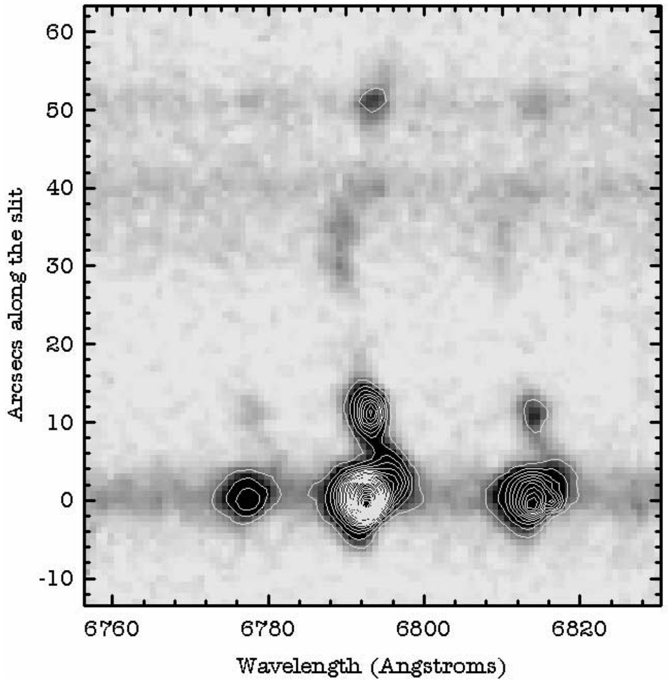

FIG. 3.—Long-slit spectrum of Arp 194, at P.A. ≈ 145°, in the range covering Hα and [N II] λλ6548, 6583. Abscissa is observed wavelength in angstroms; ordinate is arcseconds along the slit (northwest to the top). The light contour levels are meant to emphasize the line structure in the inner few arcseconds of A194S.

4. Several features of A194N, which can be ascribed to a collisional ring, as discussed below.

Following the collision interpretation we might expect Arp194 to show features predicted by models for off-center interpenetrating encounters including: (1) a prominent outer ring and (2) displacement of mass toward the ring (Gerber, Lamb, & Balsara 1992; see also the *K* images of several ring galaxies in Appleton & Marston 1997). A194N can be interpreted as a distorted ring galaxy although tracing the outer ring is not easy. Two arcs toward the south and north can be traced unambiguously, suggesting a ring of radius $R_d \approx 17$ Kpc. The hollow region toward the southeast reinforces the collisional ring galaxy interpretation because it cannot be easily explained in other terms. Another supporting element involves the trend in radial velocities along P.A. = 145°, which can be more easily explained as the result of expansion than rotation (see § 3.3). A194S shows a larger and brighter nuclear bulge suggesting that it is an earlier morphological type (Sa–Sb?) than A194N (originally type Sc?). Two blue arclike features (Figs. 1 and 2) are displaced toward the eastern and western sides of the A194S nucleus (see also the color map). They may be signatures of a ringlike expansion wave produced by the assumed head on encounter between A194N and A194S.

Interpretation of A194N is complicated by the complex morphology on the northwestern side. Two main condensations (corresponding roughly to A194N-A and A194N-B) are visible in the *K* images. This may indicate that we are detecting the nucleus of A194N and another galaxy projected nearby (i.e., A194N plus an additional perturber). The color map reddest region to the north ($B-V \gtrsim 1$) may be associated to such a perturber. The issue requires more data but the trail of blobs suggests that A194N and A194S are the main players in this interaction. Our discussion reflects that assumption.

3.2. *Emitting Regions*

Table 3 presents line fluxes for emission-line regions isolated along the slit.

3.2.1. *The Nucleus of A194S ≡ A194S-A*

The intruder nucleus is a luminous Hα source [L(Hα) ≈ 2 × 10^{41} ergs s^{-1}) with color index $B-R \approx 0.5$. The ratio I([N II] λ6584)/I(Hα) ≈ 0.4 (Figs. 4 and 5) suggests that there is no significant source of ionization other than hot stars. The moderate I([S II] λλ6716, 6731)/I(Hα) ratio (≈0.3) and very low I([O I] λ6300)/I(Hα) ratio (≈0.02) support this conclusion. A further confirmation comes from the I([O III])λ 5007/I(Hβ) ratio (≈0.8) measured by Metlov (1980). Line ratio diagnostic diagrams (Veilleux & Osterbrock 1987) show that A194S is located very close to the H II zone. Our data show no evidence for nonthermal nuclear activity. In this respect, it is worth noting that there is (Fig. 4) no variation of the I(Hα)/I([N II] λλ6548, 6583) ratio along the slit (an increase would be expected if a nonthermal contribution were present). The ratio I(Hα)/I(Hβ) measured by Metlov (1980) 3.7 : 1.0 suggests moderate extinction [$E(B-V) \approx 0.2$]. The heliocentric $v_r \approx 10{,}502$ km s^{-1} agrees with Metlov's (1980) determination within 10 km s^{-1}.

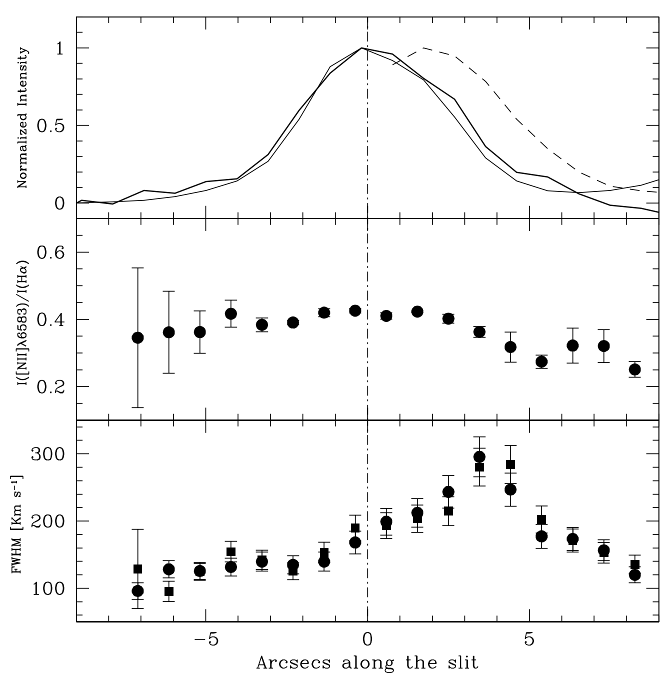

FIG. 4.—*Top*: Cross-dispersion intensity profile for Hα emission (*thin solid line*), continuum (*thick solid line*; assumed to peak at the abscissa 0 point), and extended Hα component (*dashed line*). Ordinate is intensity normalized to peak value. The extended Hα component peaks approximately 2″ from the continuum, and it is barely visible in the strip of maximum continuum emission (see also Fig. 3). *Middle*: Intensity ratio of the Hα and [N II] λ6583 lines, as a function of the distance from the nucleus of A194S. *Bottom*: for FWHM(Hβ) (*filled circles*) and FWHM([N II] λ6583) (*filled squares*) vs. distance from the nucleus of A194S. Ordinate is FWHM in km s^{-1} corrected for instrumental profile.

TABLE 2

MULTIFREQUENCY DATA FOR THE ARP 194 SYSTEM

Galaxy	Region ID	$H\alpha$+[N II][a] (ergs s^{-1} cm^{-2})	B	R	$B-R$	J[b]	K[b]	f_ν(1.4 GHz) (mJy)
A194S	Total[c]	2.29E-13	15.17	14.39	0.78	14.22	12.67	$\gtrsim$5.35
A194S	Nucleus[e]	7.94E-14	16.31	15.84	0.47	15.6	13.94	4.4[d]
Arp 194	Blob A[e]	6.26E-14	18.34	17.87	0.47	>18.35[f]	>16.35[f]	2.79
Arp 194	Blob B[e]	2.17E-14	18.18	18.06	0.12	>18.35[f]	>16.35[f]	...
Arp 194	Blob C	1.41E-14	17.98	17.72	0.26	>18.35[f]	>16.35[f]	...
A194N	Total	1.38E-13	14.37	13.58	0.79	13.88	12.11	>0.40
A194N	A194N-A " nucleus "[e]	$\lesssim$2.13E-14[g]	17.11	16.05	1.06	15.94	14.26	0.40
A194N	A194N-B	1.38E-14	17.51	16.34	1.17	15.51	13.62	...
A194N	Blob D	...	18.04	17.36	0.68	...	...	...
A194N	Arc spot A	1.10E-14	18.25	17.87	0.38	...	...	...
A194N	Arc spot B	7.14E-15	17.96	17.38	0.58	...	...	...
A194N	Arc spot C	9.61E-15	18.03	17.15	0.88	...	...	...

[a] The [N II] λ6548 line falls right at the border of the employed narrowband filter; however, considering that I([N II] λ6583)/ $I(H\alpha) \approx 0.4$ almost everywhere, this implies that the $H\alpha$+[N II] $\lambda\lambda$6548, 6583 fluxes should be corrected by $\lesssim$10% (below our estimated uncertainties even for the brightest $H\alpha$-emitting regions). No correction was applied to the values reported in this table.

[b] Near-infrared photometry by Bushouse & Stanford 1992.

[c] Excluding blobs.

[d] Value measured on FIRST with an aperture of 5''4.

[e] Emitting region covered fully or in part with long-slit spectroscopy (see Table 3).

[f] Regions not visible in the isophotal contour map by Bushouse and Stanford 1992. The lower limit to the magnitude has been estimated from the lowest level isophote plotted by Bushouse and Stanford 1992, which are $\sigma \approx 20.5$ and 18.5 mag $arcsec^2$ for J and K band, respectively. With a scale 1''35 $pixel^{-1}$, the magnitude of a very faint object contoured in a square of 1 pixel of radius would lead to $m \approx -2.15 + \sigma$.

[g] $H\alpha$ measured on a larger area than B and R.

TABLE 3

EMISSION-LINE REGIONS IN ARP 194S

Galaxy	Region ID	P.A. (deg)	v_{rHel} (km s^{-1})	[N II] λ6548 Flux[a]	W[b]	FWHM[c]	$H\alpha$ Flux[a]	W[b]	FWHM[c]	[N II] λ6583 Flux[a]	W[b]	FWHM[c]	[S II] λ6716 Flux[a]	W[b]	FWHM[c]	[S II] λ6731 Flux[a]	W[b]	FWHM[c]
A194S	A Nucleus[d]	145	10,502 ± 3	8.4	24	170	64.5	170	170	26	68.5	170	11.9	33.6	220	8.4	24	220
A194	Blob A[e]	145	10,532 ± 7	1.2	...	140	15.6	...	$\lesssim$110	3.61	...	110	2.1[f]	...	200:	1.6	...	110
A194N	A " Nucleus "[g]	145	10,435:[h]	...	...	...	0.46	5	250	0.27	3	250	...	...	...	...	...	...
A194N	A " Nucleus "[g]	118	10,430 ± 20	...	...	...	0.84	8.3	160	0.6	6.6	220	...	...	...	...	...	...

[a] Observed flux in units of 10^{-15} ergs s^{-1} cm^{-2}, uncorrected for redshift and internal extinction. Note that the correspondence between the long-slit emitting regions and the regions measured on the narrow- and broadband images labeled with the same name is rather rough (it can be checked in Fig. 1 where the slit position is marked).

[b] Equivalent width in angstroms.

[c] FWHM in kilometers per second corrected for instrumental broadening ≈2.5 Å FWHM.

[d] Only on this region a test on the accuracy of the spectra flux calibration can be done comparing the flux of the nucleus of A194S with the $H\alpha$ flux measured in the narrowband image (Table 2), since the summation was done on an area of similar value (≈25 $arcsec^2$). The agreement is very good even if the apertures are of different shape.

[e] Almost no continuum; equivalent width not defined.

[f] Flux estimated from peak intensity ratio since the line profile is contaminated by a blemish.

[g] Only partially in the slit.

[h] Double-peaked $H\alpha$ and [N II] $\lambda\lambda$6548, 6583 lines. A second component, partially resolved, peaks at $v_{rHel} \approx 10{,}566$ km s^{-1}.

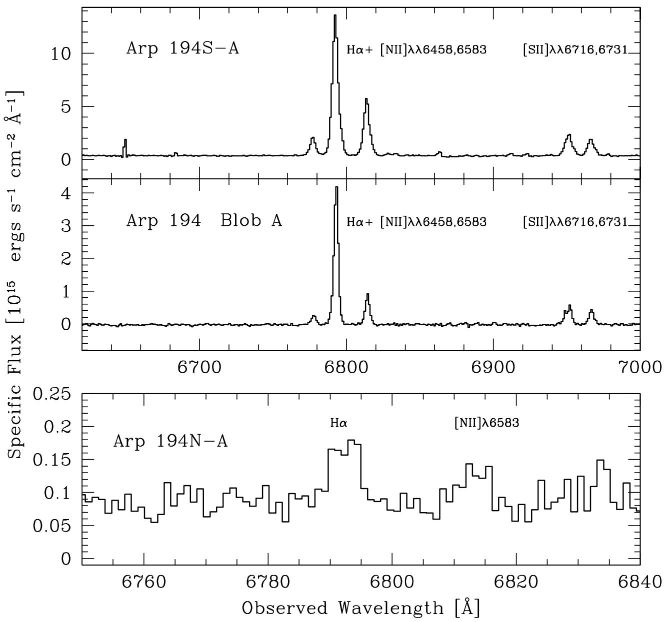

FIG. 5.—Hα spectral regions of relevant emitting line regions, ordered from the south to the north. Abscissa is observed wavelength in angstroms, ordinate is specific flux in units of ergs s^{-1} cm^{-2} $Å^{-1}$. The A194N-A spectrum (*bottom*) spectral range has been expanded, to better show the boxy and broad appearance of Hα.

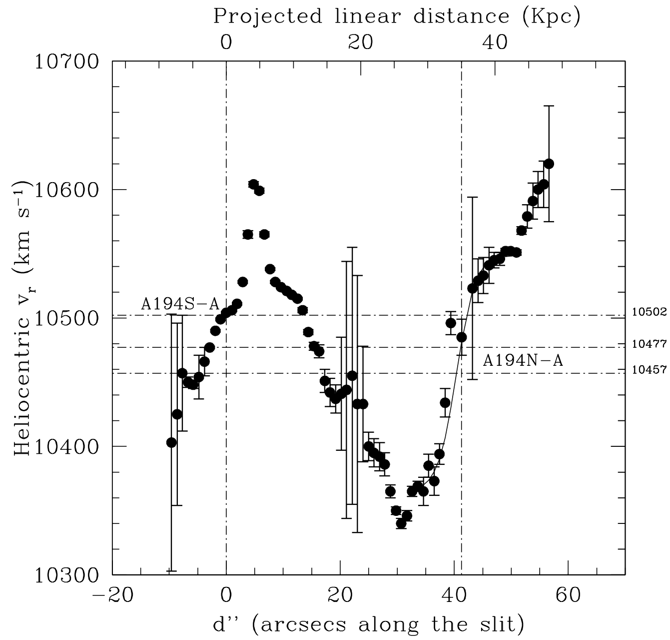

FIG. 6.—Heliocentric radial velocity curve of the Arp 194 system at P.A. = 145°. Note that the apparent discordant point at ≈40″ reflects a broadening of the Hα and [N II] $\lambda\lambda$6548, 6583 lines. The origin of the projected linear and angular distance scale has been set coincident with A194S-A (at cross-dispersion peak of the continuum). The three dot-dashed lines draw the systemic v_r measured for A194S ($v_r \approx$ 10,502 km s^{-1}) and A194N ($v_r \approx$ 10,457 and 10,477 km s^{-1}; see text for details).

3.2.2. *Blob A*

This is the second strongest source of Hα emission in the interacting pair and it is also clearly detected as a FIRST radio continuum source. Metlov (1980) measured I(O III) λ5007/I(Hβ) ≈ 1.56. The intensity ratios I(N II λ6583)/I(Hα) ≈ 0.23, I([S II] $\lambda\lambda$6716, 6731)/I(Hα) ≈ 0.24, and I(O I) λ6300/I(Hα) ≈ 0.027 indicate that H II emission is dominant, and this is confirmed by the source location in the diagrams of Veilleux & Osterbrock (1987). A ratio $L(\mathrm{H}\alpha)/\nu P_{1.4\mathrm{GHz}} \approx 800$ is a useful measure of what can be inferred about star formation processes. It is noteworthy that blob A is clearly connected to the nucleus of A194S by more extended line emission (Fig. 3; see § 3.3).

3.2.3. *A194N-A*

Source A194N-A is likely to be the nucleus of the disrupted spiral but it was only partially in the slit at both position angles. Hα and [N II] $\lambda\lambda$6548, 6583 show FWHM ≈ 250 km s^{-1}, which is approximately twice as broad as the adjacent emitting regions. The observed broadening is significant at a confidence level $\gtrsim 3\ \sigma$ taking into account a FWHM error of 15% or ≈30 km s^{-1} (1 σ). The broadening is appreciable in both spectra and it is due to the presence of an additional (redshifted) line component in the slit since the Hα and [N II] $\lambda\lambda$6548, 6583 profiles are double peaked with peak $\Delta v_r \approx$ 130 km s^{-1} (see Fig. 5, where spectra of the main emitting regions are shown). The I([N II] $\lambda\lambda$6548, 6583)/I(Hα) ratio (≈0.6) for the red component suggests the presence of nonthermal emission probably associated with shock-heated gas (not strong, otherwise the [S II] $\lambda\lambda$6716, 6731 lines would be detected).

3.3. *Radial Velocity Curves*

Figure 3 is a gray-scale reproduction of the extended Hα+[N II] $\lambda\lambda$6548, 6583 emission. The radial velocity (v_r) curve derived from this figure is shown in Figure 6 (centered on A194S-A) and in Figure 7 at P.A. ≈ 118°. Both radial velocity curves agree qualitatively with the data provided by Metlov (1980). Emission is continuous between blob A and A194S. The value v_r increases monotonically to within ≈3″ northwest of A194S-A (maximum $\Delta v_r \approx$ 120 km s^{-1}). This

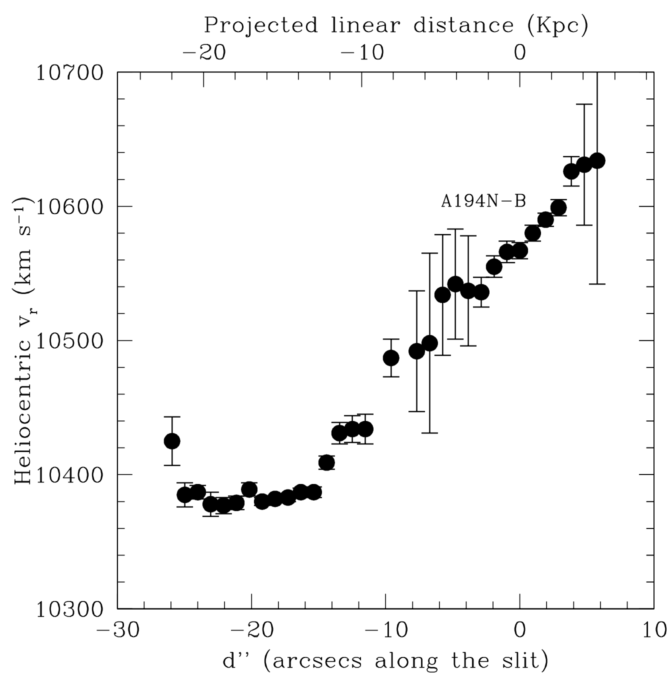

FIG. 7.—Heliocentric radial velocity curve of the Arp 194 system at P.A. = 118°. Note that, at variance with the previous figure, the origin has been set on A194N-B.

emission line component produces the cusp in the radial velocity curve between 0″–5″ from the continuum peak of A194S. The velocity curve on the northern side of A194S is obviously not due to rotational motion because it appears to turn over. The velocity cusp is most likely due to blending of the rotational velocity field with the redward-displaced component visible in Figure 3. This is made more evident by the contour overlaid on Figure 3 and by the cross-dispersion intensity profile shown in the upper panel of Figure 4. The main Hα component has been summed over -160 km s^{-1} $\lesssim \Delta v_r \lesssim$ 110 km s^{-1}; the redward component in the range 110 km s$^{-1} \lesssim \Delta v_r \lesssim$ 330 km s^{-1}. In correspondence of $\Delta d'' \approx 4''$, the total Hα emission is significantly broader since the two Hα components are blending together (the Hα profile appears double peaked).

3.4. *The Geometry and Kinematics of the Encounter*

Any inferences on the systemic v_r of A194N-A are uncertain (§ 3.2). The P.A. = 145° slit, however, crosses A194N not far from the geometrical center of the ring. Our spectrum at P.A. = 145° mainly samples the "empty" inner region of A194N. This gives us confidence that we are measuring a reasonably reliable radial velocity $v_{r,\mathrm{N}}$ for A194N at ≈41″ in Figure 6 (the edges of the ring are at 30″ and 50″, and interestingly, in their correspondence the v_r is constant over 3″). A fit to the v_r curve in this region is shown by a filled thin line in Figure 6. We derive a value $v_{r,\mathrm{N}} \approx$ 10,477 km s^{-1} if we consider the midpoint between the two segments of constant v_r; $v_{r,\mathrm{N}} \approx$ 10,457 km s^{-1} if we consider the average v_r between the two segment. The roughly symmetric appearance of the radial velocity curve around this point reinforces our confidence that $v_{r,\mathrm{N}} \lesssim$ 10,500 km s^{-1}. We derive from the observed continuum peak (the zero point of Fig. 6) $v_{r,\mathrm{S}} \gtrsim$ 10,502 km s^{-1}. Therefore, A194S is receding from A194N with $\Delta v_{r,\mathrm{coll}} \approx$ 25–40 km s^{-1}.

We conclude that A194S is more distant and this implies that the motion of the blobs relative to it follows straightforwardly. Blob A, in the two-dimensional spectrum of Figure 3 is connected to the emission line component of increasing v_r detected up to a few arcseconds from the continuum peak. The Δv_r between A194S-A (v_r measured at continuum peak) and blob is still positive ($\Delta v_r \approx$ 30 km s^{-1}). Therefore, blob A cannot be the product of outflow for the obvious reason that it would be moving in the wrong direction. *If the blobs trail A194S, blob A—as well as the extended emitting gas of increasing v_r in between blob A and A194S-A—must be falling toward A194S-A.* The validity of this results is based on two considerations: (1) the blobs, and blob A especially, trail after A194S; (2) $\Delta v_{r,\mathrm{coll}} \gtrsim$ 0 km s^{-1}, implying that A194S is further from us than A194N. In this case blob A is closer to us than A194S. We must remark that, albeit that $\Delta v_{r,\mathrm{coll}}$ is small, $\Delta v_{r,\mathrm{coll}} \lesssim$ 0 km s^{-1} is inconsistent with the v_r curve and the geometry of the system (see Fig. 6).

3.4.1. *Ring Age and Time after Crossing*

To estimate the time after crossing, we can consider that, in the special case of a head-on encounter in which the direction of motion of the intruder is strictly perpendicular to the plane of the target galaxy, the distance between the intruder and the target galaxy can be deprojected once the inclination of the target galaxy is known (this may not be strictly true for Arp 194; this is just a first approximation). The main underlying assumption is that the ring starts to expand at the time the intruder nucleus was interpenetrating the disk of the target, as suggested by theory and numerical simulations (Lynds & Toomre 1977). The expansion velocity will be $v_{\mathrm{exp}} = R_d/d_p \Delta v_r \tan i \approx 25 \Delta v_{r,\mathrm{col\,1,50}} \tan i$ km s^{-1}. The time after crossing is $\tau = R_d/v_{\mathrm{exp}}$. We can estimate the inclination of the ring making two extreme choices: (1) the northwest end is traced by the arc spots A, B, C; (2) the northwest end is the fainter spot ≈5″ to the northwest from the arc. Since this implies $54° \lesssim i \lesssim 75°$, we obtain 2×10^8 yr $\lesssim \tau \lesssim 6 \times 10^8$ yr, if $\Delta v_{r,\mathrm{coll}} = 40$ km s^{-1}. If $i = 64\overset{\circ}{.}5$, $\tau \approx 4 \times 10^8$ yr.

3.5. *Star Formation Properties*

The total Hα luminosity of the Arp 194 system is $\approx 1.5 \times 10^{42}$ ergs s^{-1}. This yields a star formation rate $\approx 10\ M_\odot$ yr^{-1} for masses between 0.1 and 100 $M_\odot$, assuming a Salpeter initial mass function (see Kennicutt 1998 for relationships and references). This value is comparable to the one of powerful starburst galaxies.[5] It is interesting to note that, if we consider the tight FIR-radio correlation of star-forming systems (Sanders & Mirabel 1996) with logarithmic index $q = 2.35$, $\log L_{\mathrm{FIR}} \approx 14.92 \log P_\nu$, we obtain $L_{FIR} \approx 2.3 \times 10^{44}$ ergs s$^{-1} \approx 6 \times 10^{10}\ L_\odot$. Arp 194 may be well a luminous *IRAS* galaxies. A vigorous star formation going on in the produced ring seems to be a common property of ring galaxies (Marston & Appleton 1995). Optical images often show a compact off-center nucleus surrounded by a number of blue knots that are H II regions. The ring component often hosts giant molecular complexes, and its color is consistent with a very young stellar population. Indeed, the ring arcs of A194N stand out in the color map since they are bluer than the surrounding regions.

3.5.1. *Is It Just a Starburst?*

A starburst surrounding the nuclear region, as well as infall of gas from above the galactic plane may produce extinction to the point to fully obscure an active galactic nucleus (AGN). Actually, the early stages in the life of an AGN may be dominated by obscuration, so that even the very AGN detection may be troublesome. This seems to be true over a wide range of luminosity, from ultraluminous far IR galaxies ($L_{\mathrm{FIR}} \sim 10^{12}\ L_\odot$), down to the nearest Seyfert 2 (see, e.g., Krongold et al. 2002; Maiolino et al. 2000; Dultzin-Hacyan 1995; Sanders et al. 1988). We computed the $L(\mathrm{H}\alpha)/\nu P_\nu$ at $\nu = 1.4$ GHz as a function of the aperture radius for increasing apertures from 2″ to 9″. In this interval the ratio is $L(\mathrm{H}\alpha)/\nu P_\nu \approx 2200$, with a ±10% change along different aperture sizes. The nuclear value is larger than the value observed on blob A (see below). Blob A is not strictly a galaxy and most likely lacks the deep potential well associated to the nuclei of galaxies where massive black holes are thought to be present. Furthermore, both the nucleus and blob A obey to the correlation between f(Hα+[N II] $\lambda\lambda$6548, 6583) and radio f_ν at 20 cm found by Kennicutt (1983) for spiral galaxies, which implies f(Hα+[N II] $\lambda\lambda$6548, 6583)$/\nu f_\nu \approx 1500$. This suggests no contribution from an obscured active galactic nucleus in A194S-A.

Having ascertained that most of the Hα and radio emission is due to H II regions, we can deduce several parameters related to star formation reported in Table 4. We will focus

[5] Unfortunately, Arp 194 has not been covered by *IRAS* observations.

TABLE 4
STAR FORMATION RESULTS FOR THE ARP 194 SYSTEM

Galaxy	Region ID	M_B[a]	$L(\mathrm{H}\alpha)$ (ergs s^{-1})	SFR[b] ($M_\odot$ yr^{-1})	$Q(\mathrm{H})$[c] (s^{-1})	$N(\mathrm{OB})$[d]	$\mathscr{M}_{\mathrm{tot}}$[e] ($M_\odot$)
A194S	Total	−21.05	5.7×10^{41}	4.5	4.8×10^{53}	100000	1.8×10^7
A194S	A nucleus	−19.91	2.0×10^{41}	1.6	1.7×10^{53}	34000	6.3×10^6
A194	Blob A	−17.88	1.6×10^{41}	1.2	1.3×10^{53}	27000	5.0×10^6
A194	Blob B	−18.04	5.4×10^{40}	0.4	4.6×10^{52}	9000	1.7×10^6
A194	Blob C	−18.24	3.5×10^{40}	0.3	3.0×10^{52}	6000	1.1×10^6
A194N ...	Total	−21.85	3.4×10^{41}	2.7	2.9×10^{53}	60000	1.1×10^7
A194N ...	A " nucleus "	−19.11	5.3×10^{40}	0.4	4.5×10^{52}	9000	1.7×10^6
A194N ...	B	−18.19	3.4×10^{40}	0.3	2.9×10^{52}	6000	1.1×10^6
A194N ...	Blob D	−18.18	...[f]	...	...	...	...
A194N ...	Arc spot A	−17.97	2.7×10^{40}	0.2	2.3×10^{52}	5000	8.7×10^5
A194N ...	Arc spot B	−18.26	1.8×10^{40}	0.15	1.5×10^{52}	3000	5.7×10^5
A194N ...	Arc spot C	−18.19	2.4×10^{40}	0.2	2.0×10^{52}	4000	7.63×10^5

[a] Blue absolute magnitude M_B.
[b] Total SFR from 0.1 to 100 $M_\odot$ computed for a Salpeter IMF from $L(\mathrm{H}\alpha)$: SFR $\approx 7.9 \times 10^{-42}$ $L(\mathrm{H}\alpha)$ $M_\odot$ yr^{-1} (Kennicutt 1998).
[c] The number of ionizing photons $Q(\mathrm{H})$ has been computed from $L(\mathrm{H}\alpha)$ following case B of nebular theory, assuming $T_e \approx 10{,}000$ K and no photon escaping the nebula.
[d] Number of OB stars, i.e., stars in the mass range 10–100 $M_\odot$, computed from $Q(\mathrm{H})$ assuming a relationship between each star $Q(\mathrm{H})$ and mass from Kurucz's models (A. Bressan 2002, private communication), and a Salpeter IMF.
[e] Total mass of IMF stars from 0.1 to 100 $M_\odot$ assuming a Salpeter IMF.
[f] Very faint Hα emission.

on blobs A and B for which we have a more complete data set. The absence of any J and K counterparts for the blobs (Bushouse & Stanford 1992) readily suggests that, if the blobs are associated to star-forming regions, their age must be relatively young and that mainly gaseous matter has been stripped through the encounter.

3.5.2. " *First Generation* " *of Stars in Blob A?*

If we were observing a very young population (i.e., a first generation of stars in which *all* stars are still in the main sequence with a total mass reported in col. [7] of Table 4), radio emission should be due exclusively to thermal bremsstrahlung in the H II regions. In this case the emissivity ratio between Hα and radio specific flux is dependent only on the electron temperature T_e (Osterbrock 1989, pages 80, 88, 95). Assuming $T_e \approx 10^4$ K, we obtain that the expected ratio at $\nu = 1.4$ GHz is $j_{\mathrm{H}\alpha}/\nu j_\nu \approx 44{,}000$ for optically thin free-free emission. This value is most likely an underestimate because the emitting region should be optically thick at 1.4 GHz: H II regions have frequently a turnover frequency between the optically thick and thin regime at $\approx$3 GHz. Since the observed ratio is more than an order of magnitude smaller, we conclude that radio emission must be mainly due to a nonthermal sources associated to supernovae. The " first-generation " scenario is not supported by the optical properties either. We computed the numbers of ionizing photons needed to sustain the $L(\mathrm{H}\alpha)$, and hence the number of OB stars (spectral type earlier than B9) under the assumption that no photon escapes from the nebulae. Approximately 30,000 OB stars are needed for blob A. However, a larger number of OB stars would be needed to account for the B absolute magnitude ($M_{B,\mathrm{blobA}} \approx -17.9$), implying that star formation has been going on beyond the main sequence lifetime of OB stars. Population synthesis calculations using STARBURST99 (Leitherer et al. 1999) confirm this suggestion. In Figure 8 the dot-dashed line shows the spectral energy distribution expected for a star cluster of total mass 5×10^6 $M_\odot$, with a Salpeter IMF predicted by STARBURST99. Emission from such star cluster fails to reproduce the observed luminosity of blob A.

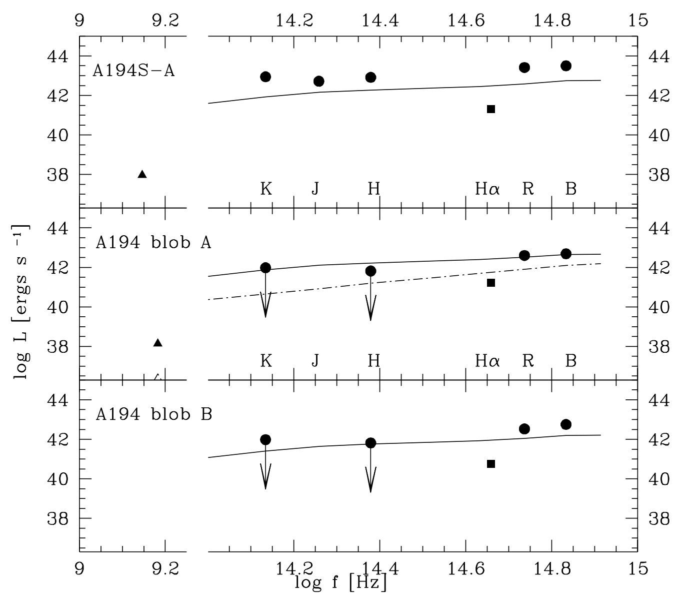

FIG. 8.—Photometric properties of A194S-A, blob A and blob B, and population synthesis. Abscissa is logarithm of frequency in hertz, ordinate is logarithm of νL_ν in ergs s^{-1}. The filled squares represent the Hα luminosity. The solid line shows the prediction of STARBURST99 simulations for the continuous SFR as reported in the fourth column of Table 4: 1.55, 1.2, 0.42 $M_\odot$ yr^{-1} for A194S-A, blob A, and blob B, respectively, after a time $\approx 7 \times 10^7$ yr. Errors are approximately the size of the symbols or smaller. The dot-dashed line of the middle panel is a simulation for the " first generation of stars " hypothesis (see text) with a main-sequence total mass $\mathscr{M}_{tot} \approx 5 \times 10^6 M_\odot$. The triangles refer to the expectation for radio power in case of only free-free emission. No correction for external extinction has been applied.

3.5.3. *Population Synthesis*

We simulated blob A and blob B as star-forming systems with SFR $\approx 1.22\ M_\odot\ \mathrm{yr}^{-1}$ and SFR $\approx 0.42\ M_\odot\ \mathrm{yr}^{-1}$, respectively [estimated from $L(\mathrm{H}\alpha)$ and as reported in Table 4], using STARBURST99. In Figure 8 we plot the luminosity in the bands for which we have available data (uncorrected for internal extinction), along with the results of STARBURST99 simulations (*solid lines*). A reasonable fit to the observed colors and to the absolute B magnitude of blob A is obtained for constant star formation rate and an age of 7×10^7 yr. This implies that the mass of the blob is $M_{\mathrm{blobA}} \gtrsim 10^8\ M_\odot$ (a lower limit since we do not know how much of gas mass belongs to the blob). We are able to reproduce the total blob A luminosity within a starburst age significantly lower than the time lapsed after A194S and A194N crossing. Not surprisingly, this is not possible for A194S-A, the nucleus of A194S: if $\mathrm{SFR_{A194S\text{-}A}} \approx 1.55\ M_\odot\ \mathrm{yr}^{-1}$, after 7×10^7 yr a star-forming system would be less luminous than A194S by a factor $\approx$10 in the K band. This implies that *the tidally stripped matter making blob A was, in origin, predominantly gaseous*.

3.5.4. *The Supernova Rate from Radio Properties: Evidence of Substantial Obscuration*

Radio emission in star-forming galaxies is expected from three major sources: (1) radio supernovae (RSNe), (2) supernova remnants (SNRs), and (3) cosmic-ray electrons injected through the Fermi acceleration mechanism in the interstellar medium (see, e.g., Condon 1992 for an excellent review). We can write the emitted power as a function of time as $P = \Sigma_k \int_{t_{\mathrm{min},k}}^{t_{\mathrm{max},k}} dn(t)/dt P_k(t) dt$, where the integration in summed over the three main radio emission mechanisms and $dn(t)/dt$ is the number of supernovae per year, and we assume that the age of the starburst is longer than the maximum $t_{\mathrm{max}} \sim 10^7$ yr (see below).

A notable example of radio-emitting supernova has been the RSN (with a type Ibc progenitor) discovered in the circumnuclear starburst region of NGC 7469, a Seyfert 1 galaxy (Colina et al. 2001). The conditions of NGC 7469 may be ultimately similar to the ones of A194S-A. However, unless a starburst is extremely young, RSNe due to Type II events should dominate the radio luminosity contribution due to SNe. We consider as representative one of the best-studied cases, SN 1979c in M100. The luminosity is an order of magnitude less than RSN NGC 7469, $\nu P_\nu \approx 5 \times 10^{36}$ ergs s^{-1}, and the light curve can be modeled as flat for a time $t_{\mathrm{max},1} \approx 2$ yr with a sharp rise and steep decline (see also Yin & Heeshen 1991; Mioduszewski, Dwarkadas, & Ball 2001). This seems to be, at present, a reasonable albeit rough assumption. The contribution due to SNR, $P_{\nu,\mathrm{SNR}}$ is a strong function of time. The SNR diameter depends on time as $D = 4.3 \times 10^{-11} (E_0/n_{e,\mathrm{int}})^{1/5} t^{2/5}$, where D is in parsecs and t in years (Clark & Caswell 1976; see, e.g., Ulvestad 1982) up to a $t_{\mathrm{max},2} \approx 10^5$ yr. E_0 is the total energy of a SN, and $n_{e,\mathrm{int}}$ is the electron density of the circumstellar medium ($n_{e,\mathrm{int}} \sim 1$ cm^{-3}). It is usually assumed that $E_0/n_e \sim 10^{51}$ ergs cm^3. We consider the observational surface brightness Σ versus D relationship in the form $\Sigma \approx 10^{-15} D^{-3}$ W m^{-2} Hz^{-1} sr^{-1} (Ulvestad 1982 and references therein). Assuming a power-law index 0.8 typical of type II SNe (Weiler et al. 1986; Colina et al. 2001, and references therein), we obtain that the total power emitted at 1.4 GHz by a SNR as a function of time is $\nu P_{\nu,1.4,\mathrm{SNR}} \approx 1.3 \times 10^{35} t^{-2/5}$ ergs s^{-1}. A third term is due to relativistic electrons injected by supernova shocks in the interstellar medium. These "cosmic-ray" electrons are thought to account for $f = 90\%$–94% of the total radio power output from a supernova remnant (Condon 1992; Bressan, Silva, & Granato 2002), and may radiate for $t_{\mathrm{max},3} \lesssim 10^7$ yr.

Assuming $dn(t)/dt$ independent on time, we obtain a rate $dn/dt \sim 2(1-f) \sim 0.1$–$0.2$ SNe yr^{-1} for the nuclear region, and $\sim 1(1-f) \approx 0.05$–0.1 SNe yr^{-1} for blob A. The SN rate deduced from radio power is in any case much larger than the value expected from stellar population synthesis, which predicts $dn(t)/dt \approx 0.015$ SNe yr^{-1} for the nuclear regions of A194S, and $dn(t)/dt \approx 0.01$ SNe yr^{-1} for blob A. The SN rate deduced from radio is $\sim$5–10 times larger than the SN rate deduced from optical properties. This hints at (1) the presence of an AGN, which may significantly affect the total power of A194S; however, this does not seem the case since the ratio between optical and radio SN rate on A194S-A is similar to that of blob A; at (2) obscuration; (3) a short-lived ($\sim 10^7$ yr), poststarburst phase in which the ratio SFR$/\nu P_\nu$ reaches a minimum (Bressan et al. 2002). This is predicted for an impulsive starburst, and is due to the strong enhancement of the radio emission following the supernova explosion of the lowest-mass Type II supernova progenitors (which are also the most frequent for standard IMFs). Obscuration is most likely to play the major role. Especially in systems such as the nuclear regions of A194S and blob A, which are spheroidal in appearance, Hα emission may be detected only from the star-forming regions nearer to be observer. The SFR measured from the FIR luminosity is $\gtrsim$10 times larger than the SFR measured from Hα (Kennicutt 1998). The rate of SNe found from a search in the K band is also a factor $\sim$5–10 larger than the rate estimated from optical surveys (Maiolino et al. 2002; Mannucci et al. 2003).

4. DISCUSSION

4.1. *Cross-Fueling in Interpenetrating Encounters*

Numerical simulations of head-on collisions between galaxies show that a substantial mass of gas is "splashed out" into a bridge connecting the two centers of potential. After the collision the gas is reaccreted either from the intruder and from the primary disk. The amount of material pushed out in the collision depends on the relative orientation and impact parameter of the encounter. The subsequent infall is spatially asymmetric and is primarily located in a well-defined streams. Most of the accreted gas ends up in the central regions of the model galaxies (Struck 1997). However, cross-fueling is definitely not an easy phenomenon to prove observationally. In the framework of a galaxy pair, it implies three physical requirements: (1) that gas is stripped from one galaxy; (2) that the gas, stripped from one galaxy, is falling toward the other; (3) that the infalling gas is actually fueling a starburst or an AGN. These three conditions may be met only in very special systems, and may be demonstrable in many fewer. At least, in the case of collisional ring galaxies systems like Arp 194 it is easy to test whether cross-fueling is indeed occurring. First, the blob and the morphology of A194N provide evidence in favor of stripping. The second condition is also satisfied with reasonable certainty *for blob A* (nothing can be said on blob B and C). On blob A we are observing Hα and [N II] $\lambda\lambda$6548, 6583 line components whose redshift is increasing as the gas is approaching the nucleus of A194S. The third condition is also met, since the SFR $\approx 4.5\ M_\odot\ \mathrm{yr}^{-1}$ for A194S-A and total SFR $\sim 10\ M_\odot\ \mathrm{yr}^{-1}$ are typical for estimates of SFR from Hα luminosity in starburst galaxies.

The emission line feature observed between blob A and A194S in the spectrum at P.A. = 145° is not unlike the one observed in NGC 7592, in which the two interacting galaxies are much closer, and in which a bright Hα filament connects the nuclei of the two components (Rafanelli & Marziani 1992; Marziani et al. 2001). Interpenetrating encounters lead to some easily demonstrable cases of tidal stripping. Al least two other cases have been studied in detail, Kar 29 and ESO 253-IG026 (Marziani et al. 2001, 1994). ESO 253-IG026 shows an impressive, bright filament connecting the two galactic components. Evidence of cross-fueling has been collected in other galactic pairs, especially in mixed spiral/elliptical pairs in which a starburst has been induced in the early type component: for example, in AM 0327−285 (de Mello et al. 1995, 1996), and in Arp 105 (Duc et al. 1997; see also Domingue 2001). We can study more easily some systems containing a collisional ring galaxy since they are at a special timing after contact and oriented favorably. Even if the conditions are special, they provide a laboratory to study accretion gas flows on 100 pc to kiloparsec scales, which cannot be obtained as easily in more complex systems like most merging systems.

4.2. *Tidal Stripping, Tidal Dwarf Galaxies, and the Superwind Phenomenon*

Albeit the blob B and C look slightly fainter than A, it is conceivable that they may be of comparable mass. The total mass of the blobs can therefore be several $10^8\ M_\odot$. The ejection of stellar and gaseous material into the intergalactic medium and its subsequent rearranging may lead ultimately to the formation of self-gravitating tidal dwarf galaxies (Duc et al. 2000). In this respect it is interesting to note that the mass of blob A is within the range of dwarf galaxies.

The Arp 194 system shows that a part of the orbital energy can be transferred to the gas motion (e.g., Marziani et al. 1994 in the case of Kar 29; Horellou & Combes 2000) in the special case of a collisional ring galaxy. This is expected in general from simulations of interacting galaxies. Orbital energy transfer leads to vertical motions of gas from a system that, when unperturbed, was dynamically very cold with a very low vertical velocity dispersion. Filamentary structures emerging from disk and dwarf galaxies are a telltale signature of superwinds (see for instance the spectacular case of NGC 1808; Phillips 1993). Superwinds are currently explained as due to the kinetic energy injected by stellar winds and SNe around compact starburst regions (e.g., Heckman, Lehnert, & Armus 1993; Heckman 2002). This explanation neglects the observational fact that the wide majority of superwind galaxies belong to strongly interacting systems (Marziani & Dultzin-Hacyan 2000). A rather large fraction of superwind galaxies (possibly nine out of 20, of which three with obvious evidence of tidal stripping) were found in merging systems. Small companions, leading to appreciable perturbations, were also seen near approximately one-third of the superwind galaxies. Also in the case of minor mergers the velocity dispersion in the inner disk is expected to be significantly increased and the disk structure to become unstable (Walker, Mihos, & Hernquist 1996). Implications of ongoing interactions—and of gravitationally induced, nonrotational gas motions—have not been taken into account in the theory of galactic superwinds. Even if it is possible to obtain a momentum and energy flow consistent with the observed superwind properties from the mass ejections by stellar wind and SNe (Leitherer et al. 1992), several superwind aspects—including the possibility that the wind matter could escape from the galactic potential well—could be influenced if the out-of-disk flow is eased by tidal forces, since most superwind flows are apparently only "marginally bound" (Martin 1999). There could be important consequences for the enrichment of any intracluster medium. We know the relative velocity Δ_V between blob A and A194N-A. We can estimate the kinetic energy of tidally stripped matter as $E_k = \frac{1}{2} M_{\mathrm{blob}} \Delta v^2 \approx 2.5 \times 10^{54} M_8\ \Delta v_{50}^2$ ergs. The E_k imparted to blob A corresponds to the total kinetic energy produced by $\sim 10^3$–10^4 SNe, and it may be still a small fraction of the total superwind energy ($\sim 10^{55}$–10^{57} ergs, which corresponds to the total output of 10^4–10^6 supernovae). However, gravitational forces could have still an important impact. E_k could easily be much higher, since Δv imparted to the streaming gas could be much larger than the one assumed on the basis of blob A observations and the blob mass could well be much larger than estimated. The kinetic energy value for tidally stripped matter and superwind outflow can therefore become comparable. We have shown that at least blob A and B can be thought as being entirely gaseous in origin. The relevance of Arp 194 to the superwind phenomenon is that it demonstrates observationally that gas motions can be perturbed to the point of giving rise to a stream perpendicular to the galactic plane because of gravitational acceleration.

There are other examples of a superwind-like outflow manifestly driven by interactions. Kar 29 is likely to be the result of a high velocity encounter ($\Delta v_r \approx 1000$ km s^{-1}) between an early-type galaxy (the northern component) and a late-type spiral (see Hearn & Lamb 2001 for a review of observational data on this object). The stripped gas emerging from the spiral southern component has not been captured by the elliptical and may be instead falling back toward the spiral as in a true "galactic fountain." Fraternali et al. (2001) found that the galactic-fountain H I motions in the spiral NGC 2403 are difficult to explain in the pure superwind scheme without accounting for interactions. Also, van der Hulst & Sancisi (1988) suggested that the high-velocity H I gas moving at high speed perpendicular to the disk of M101 could be explained in term of a collision between a large gas mass and the disk of M101 itself. Similarly, some high velocity clouds observed in our Galaxy are likely due to tidal effect related to the crossing of the Galaxy by the Large Magellanic Cloud (e.g., Wakker & van Woerden 1997). These findings can be understood through the simulations mentioned in the introduction. We conjecture that, in mergers and in minor mergers, there could be an important effect of gravitational forces on gas motion perpendicular to the original disk plane.

5. CONCLUSION

We have analyzed in detail the photometric properties and the kinematics of the strongly interacting system Arp 194. The main constituents of this system are a collisional ring system (A194N) and an intruder (A194S) that have experienced an interpenetrating, head-on encounter a few 10^8 yr ago. We have shown that tidally stripped gas is falling toward the center of the intruder, A194S, and that it is fueling a strong nuclear and circumnuclear starburst. Arp 194 is therefore one of the few known objects for which convincing evidence of cross-fueling exists. Considering that gas is usually confined in a " dynamically cold " configuration in disk galaxies, the Arp 194 case indicates transfer of orbital energy to the internal motion of gas during the encounter. We suggest that gas motions in superwind galaxies—which are mostly interacting systems—could also be affected by the same mechanism.

Several aspects of the Arp 194 system deserve further scrutiny. The morphology of A194N is fairly complex, and the distorted morphology of the ring, as well as the bright arc of A194N, indicates the possibility of perturbations by a third party. A full coverage with slit spectroscopy will allow to confirm the presence of a third intruder galaxy located approximately in correspondence of the northern side of the ring. High spatial resolution spectroscopy may reveal more complex motions in proximity of the nucleus of A194S. In the interacting galaxy pair NGC 1409/10 the ongoing mass transfer seems to follow a spiraling pattern (Keel 2000; similar considerations may apply to NGC 7592: Hattori et al. 2002). There is no indication of a hidden AGN presence from our data, but this result depends on the resolution of the FIRST survey data. It is possible that higher resolution data may reveal a high surface brightness compact core. In addition, further radio observations could detect radio supernova events: if $dn/dt \approx 0.3$ and if a radio supernova event remains detectable for $\approx$3 yr, we may even reveal one event at any observing time.

P. M. acknowledges financial support from the Italian MURST through Cofin 00-02-004. D. D.-H. acknowledges grant IN 115599 PAPIIT-UNAM. We wish to thank Alessandro Bressan for providing us with the numbers of ionizing photons as a function of stellar spectral type and Radoslav Zamanov and Massimo Della Valle for fruitful discussions.

REFERENCES

Appleton, P. N., & Marston, A. P. 1997, AJ, 113, 201
Appleton, P. N., Schombert, J. M., & Robson, E. I. 1992, ApJ, 385, 491
Appleton, P. N., & Struck-Marcell, C. 1987, ApJ, 318, 103
Arp, H. 1966, ApJS, 14, 1
Barnes, J. E., & Hernquist, L. 1992, Nature, 360, 715
———. 1996, ApJ, 471, 115
———. 1998, ApJ, 495, 187
Becker, R. H., White, R. L., & Helfand, D. J. 1995, ApJ, 450, 559
Bressan, A., Silva, L., & Granato, G. L. 2002, A&A, 392, 377
Bushouse, H. A., & Stanford, S. A. 1992, ApJS, 79, 213
Charmandaris, V., Laurent, O., Mirabel, I. F., Gallaris, P., Sauvage, M., Vigroux, L., & Cesarsky, C. 2001, Ap&SS, 276, 553
Clark, D. H., & Caswell, J. L. 1976, MNRAS, 174, 267
Colina, L., Alberdi, A., Torrelles, J. M., Panagia, N., & Wilson, A. S. 2001, ApJ, 553, L19
Condon, J. J. 1992, ARA&A, 30, 575
de Mello, D. F., Keel, W. C., Sulentic, J. W., Rampazzo, R., Bica, E., & White, R. E. 1995, A&A, 297, 331
de Mello, D. F., Sulentic, J. W., de Souza, R. E., Reduzzi, L., & Rampazzo, R. 1996, A&A, 308, 387
Domingue, D. L. 2001, Ph.D. thesis, Univ. Alabama
Duc, P. A., Brinks, E., Springel, V., Pichardo, B., Weilbacher, P., & Mirabel, I. F. 2000, AJ, 120, 1238
Duc, P.-A., Brinks, E., Wink, J. E., & Mirabel, I. F. 1997, A&A, 326, 537
Dultzin-Hacyan, D. 1995, Rev. Mexicana Astron. Astrofis. Ser. Conf., 3, 31
Fraternali, F., Oosterloo, T., Sancisi, R., & van Moorsel, G. 2001, ApJ, 562, L47
Gerber, R. A., Lamb, S. A., & Balsara, D. S. 1992, ApJ, 399, L51
Hattori, T., Yoshida, M., Ohtani, H., Ishigaki, T., Sugai, H., Hayashi, T., Ozaki, S., & Ishii, M. 2002, PASJ, 54, 393
Hearn, N. C., & Lamb, S. A. 2001, ApJ, 551, 651
Heckman, T. M. 2002, in ASP Conf. Ser. 254, Extragalactic Gas at Low Redshift, ed. J. Mulchaey & J. Stocke (San Francisco), 292
Heckman, T. M., Lehnert, M. D., & Armus, L. 1993, in The Environment and Evolution of Galaxies, ed. J. M. Shull & H. A. Thronson, Jr. (Dordrecht: Kluwer), 455
Ho, L. C., & Ulvestad, J. S. 2001, ApJS, 133, 77
Horellou, C., & Combes, F. 2000, in ASP Conf. Ser. 197, Dynamics of Galaxies: From the Early Universe to the Present (San Francisco: ASP), 351
Keel, W. C. 2000, BAAS, No. 197, 37.01
Kennicutt, R. 1983, A&A, 120, 219
———. 1998, ARA&A, 36, 189
Krongold, Y., Dultzin-Hacyan, D., & Marziani, P. 2002, ApJ, 572, 169
Leitherer, C., et al. 1999, ApJS, 123, 3
Lynds, R., & Toomre, A. 1976, ApJ, 209, 382
Maiolino, R., Vanzi, L., Mannucci, F., Cresci, G., Ghinassi, F., & Della Valle, M. 2002, A&A, 389, 84
Mannucci, F., et al. 2003, in preparation
Marston, A. P., & Appleton, P. N. 1995, AJ, 109, 1002
Martin, C. L. 1999, ApJ, 513, 156
Marziani, P., D'Onofrio, M., Dultzin-Hacyan, D., & Sulentic, J. W. 1999, AJ, 117, 2736
Marziani, P., & Dultzin-Hacyan, D. 2000, in ASP Conf. Ser. 215, Cosmic Evolution and Galaxy Formation: Structure, Interactions, and Feedback, ed. J. Franco, E. Terlevich, O. López-Cruz, & I. Aretxaga (San Francisco: ASP), 122
Marziani, P., Dultzin-Hacyan, D., Krongold, Y., & D'Onofrio, M. 2001, ASP Conf. Ser. 249, The Central Kiloparsec of Starbursts and AGN: The La Palma Connection, ed. J. H. Knapen, J. E. Beckman, I. Shlosman, & T. J. Mahoney (San Francisco: ASP), 284
Marziani, P., Keel, W. C., Dultzin-Hacyan, D., & Sulentic, J. W. 1994, ApJ, 435, 668
Metlov, V. G. 1980, Soviet Astron. Lett., 6, 110
Mihos, J. C., & Hernquist, L. 1996, ApJ, 464, 641
Mioduszewski, A. J., Dwarkadas, V. V., & Ball, L. 2001, ApJ, 562, 869
Osterbrock, D. E. 1989, in Astrophysics of Gaseous Nebulae and Active Galactic Nuclei (Mill Valley, CA: Univ. Sci.)
Owen, F. N., Spanger, S. R., & Cotton, W. D. 1980, AJ, 85, 351
Phillips, A. C. 1993, AJ, 105, 486
Rafanelli, P., & Marziani, P. 1992, AJ, 103, 743
Sanders, D. B., & Mirabel, I. F. 1996, ARA&A, 34, 749
Sanders, D. B., Soifer, B. T., Elias, J. H., Neugebauer, G., & Matthews, K. 1988, ApJ, 328, L35
Schmitt, H. R. 2001, AJ, 122, 2243
Semelin, B., & Combes, F. 2000, A&A, 360, 1096
Smith, B. J., Struck, C., & Pogge, R. W. 1997, ApJ, 483, 754
Smith, B. J., & Wallin, J. F. 1992, ApJ, 393, 544
Struck, C. 1997, ApJS, 113, 269
Struck-Marcell, C. 1990, AJ, 99, 71
Theys, J. C., & Spiegel, E. A. 1976, ApJ, 208, 650
Toomre, A. 1978, in IAU Symp. 79, The Large-Scale Structure of the Universe, ed. M. S. Longair & J. Einasto (Dordrecht: Reidel), 109
Ulvestad, J. S. 1982, ApJ, 259, 96
Ulvestad, J. S., & Ho, L. C. 2001, ApJ, 558, 561
van der Hulst, T., & Sancisi, R. 1988, AJ, 95, 1354
Veilleux, S., & Osterbrock, D. E. 1987, ApJS, 63, 295
Vorontsov-Velyaminov, B. A. 1977, A&AS, 28, 1
Yin, Q. F., & Heeschen, D. S. 1991, Nature, 354, 130
Wakker, B. P., & van Woerden, H. 1997, ARA&A, 35, 217
Walker, I. R., Mihos, J. C., & Hernquist, L. 1996, ApJ, 460, 121
Weiler, K. W., Sramek, R. A., Panagia, N., van der Hulst, J. M., & Salvati, M. 1986, ApJ, 301, 790